Afyon Kocatepe Üniversitesi Fen ve Mühendislik Bilimleri Dergisi

Afyon Kocatepe University Journal of Science and Engineering

AKÜ FEMÜBİD **21** (2021) 055701 (1167-1180) AKU J. Sci. Eng. **21** (2021) 055701 (1167-1180)

DOI: 10.35414/akufemubid.821905

Araştırma Makalesi / Research Article

A Numerical Study of Hydrogen Production via High-temperature and Low-temperature Water-Gas Shift Reactors' System: The Multi-Scale Modeling Approach and Simulation

Seçgin KARAGÖZ[1]

[1] *Department of Chemical Engineering, College of Engineering, Qatar University, P.O. Box: 2713, Doha, Qatar*

skaragoz@qu.edu.qa, ORCID ID: http://orcid.org/0000-0003-1287-7291

Geliş Tarihi: 05.11.2020 Kabul Tarihi: 26.10.2021

Abstract

The primary purpose of this study is to develop an advanced, and comprehensive multi-scale mathematical models of a packed bed reactors (PBRs) carrying out high and low temperature water-gas-shift reactions (WGSRs) for the hydrogen production. In industrial hydrogen generation applications, the water-gas-shift reactors are considered at high (called HTSR) and low (called LTSR) temperature stages with a cooling process between them. Therefore, detailed and advanced numerical studies on the HTSR and the LTSR in series are carried out to assess the overall performance of hydrogen production system. After completing a single-pellet, non-isothermal, steady-state simulation, we couple our model with a non-isothermal (adiabatic), steady-state packed-bed reactor model to form a hybrid multi-scale reactor model. The velocity, temperature and species' concentration profiles along both the reactor length and the pellet radius are captured by using rigorously defined momentum, energy, and species transport models, accounting for the physical mechanisms involved in the system such as convection, conduction, and reaction-diffusion. The model's equations are simultaneously solved for each domain: bulk gas domain and catalyst-pellet domain. The rigorous Maxwell-Stefan Model is applied on the reactor scale to account mass diffusion fluxes. On the other hand, Dusty Gas Model is considered to describe mass diffusion fluxes for the single pellet scale. Studies that include a broad range of the operating conditions and design parameters are carried out in this paper, in order to investigate the upper and lower limit conditions' effects on the results.

Keywords
CFD Simulation; Dusty Gas Model; HTSR; LTSR; Multi-scale Modelling; Maxwell-Stefan Model

Yüksek Sıcaklık ve Düşük Sıcaklık Su-Gaz Değiştirme Reaktörleri Sistemi ile Hidrojen Üretimi Üzerine Nümerik Çalışma: Çoklu-Ölçekli Modelleme Yaklaşımı ve Simülasyonu

Öz

Bu çalışmanın temel amacı, hidrojen üretimi için yüksek sıcaklık ve düşük sıcaklık su-gaz değiştirme reaksiyonlarının (WGSR'ler) gerçekleştiği dolgu yataklı reaktörler sisteminin (PBR'ler) gelişmiş ve ayrıntılı çoklu-ölçekli matematiksel modellerini geliştirip, simülasyonlarını gerçekleştirmektir. Endüstriyel hidrojen üretimi için en yaygın kullanılan yöntem yüksek sıcaklık su-gaz değiştirme reaktörünün (HTSR) düşük sıcaklık su-gaz değiştirme reaktörüne (LTSR) aralarında soğutma işlemi olacak şekilde seri halde bağlanmasıyla oluşan sistemdir. Bu nedenle, bu çalışma hidrojen üretim sisteminin davranışını tahmin etmek için seri haldeki HTSR+LTSR sistemi üzerinde ayrıntılı ve gelişmiş nümerik simülasyonların gerçekleştirilmesini amaçlamaktadır. Çalışmada tek kataliz peletinin izotermal olmayan, kararlı durum simülasyonunu tamamladıktan sonra, hibrit çoklu-ölçekli reaktör modeli oluşturmak için izotermal olmayan (adyabatik), kararlı durum dolgu yataklı reaktör modeliyle birleştirilmiştir. Hem reaktör uzunluğu hem de kataliz pelet yarıçapı boyunca hız, sıcaklık ve türlerin konsantrasyon profilleri, konveksiyon, iletim ve reaksiyon-difüzyon gibi sistemde yer alan fiziksel mekanizmaları dikkate alarak titizlikle tanımlanmış momentum, enerji ve taşınım modelleri kullanılarak elde edilmiştir. Model denklemleri her bir çalışma alanı (reaktör gaz fazı alanı ve kataliz pelet alanı) için eş zamanlı olarak çözülmüştür. Maxwell-Stefan Modeli kütle difüzyon akışlarını hesaba katmak için reaktör ölçeğine

Anahtar kelimeler
CFD Simülasyon; Dusty Gaz Modeli; HTSR; LTSR; Çoklu-Ölçekli Modelleme; Maxwell-Stefan Modeli

uygulanırken, Dusty Gaz Modeli de tek kataliz pelet ölçeği için kütle difüzyon akışlarını hesaplama da kullanılmıştır. Bu çalışmada, üst ve alt limit koşullarının sonuçlar üzerindeki etkilerini araştırmak için çok çeşitli çalışma koşullarını ve tasarım parametrelerini içeren simülasyonlar gerçekleştirilmiştir.

1. Introduction

The importance of hydrogen and hydrogen technologies have increased recently for both mobile and stationary practices due to the global green processes trend, and the capability of the hydrogen is being a crucial energy source and industrial species (Karagöz *et al.* 2018). Therefore, hydrogen has a high interest and potential to be the leading energy source for the future, especially it is applications of the fuel cell technology improvement. Fuel cell technology has gained massive global attention because of being alternative to traditional technologies for clean power generation in the recent years (Adrover *et al.* 2009, Huang and Ho 2008, Karagöz *et al.* 2020). Hydrogen is the most widespread and the ideal fuel for the fuel cell applications. However, hydrogen must be generated from nonrenewable energy sources or renewable energy sources because it does not naturally exist as a pure compound on Earth. Traditionally, hydrogen is being produced from energy sources such as coal, natural gas, biomass, and liquid hydrocarbons (Abdollahi *et al.* 2010, Garshasbi *et al.* 2017). The improvement of the hydrogen economy is the main factor that will determine the worldwide use of hydrogen. Thus, more economical hydrogen production with significant cost reduction is required for the transition to achieve these goals.

The Water Gas Shift Reaction-WGSR is a historically well-studied/known commercial chemical process, and has many very important industrial applications (Karagöz *et al.* 2019a). Among these applications, the WGSR plays a very crucial role in the H_2 production process by serving as further H_2 enrichment and CO degradation. Because of this role, the WGSR is considered as a promising route for H_2 production, so the WGSR-based H_2 generation processes have been gaining a renewed interest recently. Thus, there are significant efforts in both industry and academia to demonstrate its applications on environmentally friendly gasified coal power plants and fuel cells, and perspective applications of hydrogen as a clean energy carrier in the near future (Karagöz *et al.* 2019b). Aforementioned essential features of the WGSR in the literature are: (1) hydrogen is produced by the following moderately exothermic-reversible-equilibrium limited reaction:

$$CO + H_2O \Leftrightarrow CO_2 + H_2 \qquad \left(\Delta H^0_{298K} = -41.1\ kJ/mol\right) \quad (1)$$

(2) higher conversions are obtained at low temperatures with favorable kinetics at higher temperatures. (3) The reaction obeys the Le Chatelier's principle. (4) Since there is no change in the total number of moles in the process, the process does not influence on the equilibrium conversion. (5) The process temperature and feed composition are the two process parameters that have direct effect on the equilibrium conversion.

Most of the industrially relevant processes uses the multi-phase and multi-scale reactors to perform reactions. In these reactors types, multiple species involve in the process, so advanced models are necessary to reach success for the numerically related studies (Lim and Dennis 2012). Packed bed reactor is well-known and the most common among these reactor types. The conventional packed bed reactor-PBR models are pseudo-homogeneous and heterogeneous models (Froment 1974). To reach the desired level of accuracy on modeling and simulation, the heterogeneous models have some advantages over the pseudo-homogeneous models. The most crucial of these are solving transport model-equations individually for each phase in porous media, accounting explicitly gradients within of each phase and between phases, and satisfaction on one-dimensional reactor simulation (axial) even though being high-level dimensionality (Rout and Jakobsen 2015).

The study of the multiphase transport phenomena inside porous media is performed by a broad range of engineering disciplines (Rout and Jakobsen 2015). This is due to a high-level complication of

multiphase systems; create a complex set of problems and challenges. The most important features of these systems are having the character of the being nonlinear, and this requires a quantification of the multiple-coupled set of nonlinear differential equations for most of the problem solutions (Miller *et al.* 1998). Thus, the accurate modeling of the multiphase transport phenomena is crucial in many technological and industrial applications, involving of simultaneous heat-momentum-multi component mass transport.

This study focuses on a non-isothermal, steady state spherical pellet of catalyst and a non-isothermal (adiabatic), multi-scale (Catalyst-pellet/Reactor Scale) reactor modeling and simulation. The numerical study is performed on the WGSR for the H_2 generation. In spite of the existence of the various numerical studies relating the WGSR (Ding and Chan 2008, Francesconi *et al.* 2007, Seo *et al.* 2006, Wright and Edgar 1994), insufficient attempt in the area of the multiscale world is realized at first glance.

However, this effort provides a detailed numerical insight into the transport phenomena with multiscale studies in porous media (pellet and reactor scales) on the HTSR and the LTSR system in series. This study and multi-scale model results provide a practical realization about the WGSRs systems from the standpoint of industrial application for H_2 production. The COMSOL Multiphysics Software is used to the solution of the derived multi-scale model's equations in this study. The rigorous DGM (Dusty Gas Model) and rigorous MSM (Maxwell–Stefan Model) are used to account diffusion fluxes in the reactor and the pellet scales, respectively. In the majority of the studies in the literature, it is recognized that the simplification on the application of the DGM by considering uniformity on the catalyst pellet's temperature and pressure profiles along the radius. However, this study performs calculations to obtain the temperature and the pressure profiles along the catalyst's radius to validate the assumptions above, and the Dusty Gas Model is rigorously applied in the pellet model equations solution. Studies that include a broad range of the operating conditions and parameters are carried out in this paper, in order to investigate the upper and lower limit conditions' effects on the results.

2. Process Description and Solution Method

In general, industrial hydrogen generation applications, the water-gas-shift reactors are considered at high (called HTSR) and low (called LTSR) temperature stages with a cooling process between them. The flow of process gas stream occurs from the reformer unit through the adiabatic two-stage water gas shift reactors' system, such as Figure 1.

The HTSR is performed between the 300 °C – 450 °C, while LTSR is carried out between the 200 °C – 300 °C. For HTSR and LTSR, specific catalysts are used for each reactor types. Typically, Cu–ZnO–Al_2O_3 based catalysts (for LTSR) and Fe_3O_4 –Cr_2O_3–CuO-based catalysts (for HTSR) are used in industry (Chen *et al.* 2008, Natesakhawat *et al.* 2006). In the HTSR, rapid CO conversion is obtained (the majority of the CO is consumed in the HTSR) and then, the HTSR reactor's exit gas stream goes into an inter-stage cooling system. To convert the rest of the CO and enrich the H_2 product, LTSR process takes place following the cooling. The aforementioned H_2 production system is preferred industrially due to its capability of achieving higher CO conversions and desired level of hydrogen production.

The Packed Bed Reactors (PBRs) multi-scale mathematical models are developed (Figure 2). In this study, the PBRs are considered as micro (catalyst pellet) and macro (reactor) scale levels. All pellet characteristic parameters of average pore size, reaction kinetic rates, pellet material properties and pellet shape is modeled at micro (pellet) scale.

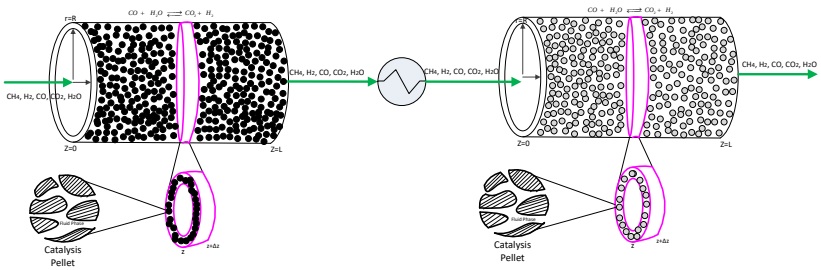

Figure 1. 1D Representation of control volumes in a two-stage process of WGSR unit.

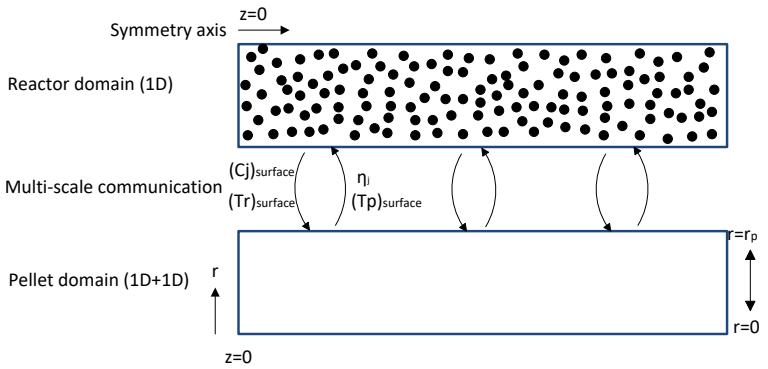

Figure 2. Representation of the Multiscale Modeling Approach.

On the other hand, macro (reactor) scale is modeled by considering reactor tube dimensions, catalyst packing void fraction, and others as all PBR features. Numerical solutions of the derived transport equations in pellet-reactor scales are obtained by coupling of these scales. Throughout the PBRs axis, the solution of the distributed catalyst pellets domains contributes as a source terms to the solution of reactor domain equations by exchanging the necessary information from the pellets' boundaries. By this multi-scale approach, reactor scale information such as pressure, temperature, velocity, and species' concentrations and pellet scale information are exchanged between these domains. At the end of this process, temperature, pressure, and species profiles are known at each axial location within the reactor domain, and at each pellet domain radial, reactor domain axial local pair. After completing the single-pellet non-isothermal, dynamic, stand-alone simulations, formed a non-isothermal, steady-state, multi-scale reactor model by coupling the single-pellet with reactor model. The solution of the catalyst pellet's equations is repeatedly performed along the reactor axis (yielding the effectiveness factor along the reactor length for the locally prevailing reaction conditions) and is coupled with a 1-D (axial) reactor model that captures species transport/reaction along the reactor. The effectiveness factor is defined as the ratio of the real rate of generation of the jth species within the catalyst pellet over the rate of production of the jth species. The conservation equations are solved by the Finite Element Method (FEM).

3. Mathematical Formulation and Modeling

In PBRs, mass-momentum-energy is constantly exchanged between the gas and solid phases that construct the catalyst and reactor scales. In this study, the Reynolds Transport Theorem is implemented individually to each of the domains, reactor scale gas-solid phases and catalyst scale gas-solid phases. The following assumptions are considered for model equations derivation; considering catalyst as a spherical shape, homogeneous porous structure of the pellet, same size of pallet forms the reactor, the gaps between the pellets are equal, the reaction does not cause any structural changes inside of the catalyst, stagnant solid-phase, active sites of catalyst are evenly distributed across the entire pellet, the assumption of being a mean pore diameter, and the ratio between the porosity and tortuosity is employed to qualify the fixed structure of the catalyst, the reaction kinetics and reaction orders

are assumed to be constant over the all performed simulation conditions, no side reaction happens, axisymmetric flow in a cylindrical tube, no radial and tangential velocities in a cylindrical tube, no diffusion throughout the reactor, negligible kinetic and potential energy terms, no heat flux by radiation, the reaction mixture does not have changing phase and ideal gas mixture is considered. For the following sections, the identification of the existing domains in reactors are the catalyst pellet: p, reactor domains: r, solid phases: s and fluid phases: f. The symbols γ and α will represent phases and domains, respectively.

The final molar based total mass conservation equations of the catalyst-pellet and reactor domains can be expressed as shown in Eq. (2) and (3), respectively. The Eq. (4) and (5) demonstrates the final molar-based species mass conservation equations for the domains of the catalyst and reactor, respectively.

Catalyst-Pellet Domain:

$$\sum_{i=1}^{\nu} \varepsilon_{s,V}^{p} \rho_{s}^{p} \bar{R}_{f,i}^{p} r^{2} = \frac{d}{dt}\left(\varepsilon_{f,V}^{p} \sum_{i=1}^{\upsilon} c_{f,i}^{p} \right) + \frac{d}{dr}\left(r^{2} \varepsilon_{f,A}^{p} \sum_{i=1}^{\upsilon} c_{f,i}^{p} \overrightarrow{v_{f}^{p}} \right) \tag{2}$$

Reactor Domain:

$$\sum_{i=1}^{\nu} \varepsilon_{s,V}^{r} \frac{A^{p}}{\varepsilon_{s,V}^{p} V^{p}} \left[\left(\varepsilon_{f,A}^{p} \overrightarrow{N_{i}^{p}} \right) \Big|^{CS^{p}} \right] = \frac{d}{dt}\left(\varepsilon_{f,V}^{r} \sum_{i=1}^{\upsilon} c_{f,i}^{r} \right) + \frac{d}{dz}\left(\varepsilon_{f,A}^{r} \sum_{i=1}^{\upsilon} c_{f,i}^{r} \overrightarrow{v_{f}^{r}} \right) \tag{3}$$

Catalyst-pellet Domain:

$$\varepsilon_{s,V}^{p} \rho_{s}^{p} \bar{R}_{f,i}^{p} r^{2} = \frac{d}{dt}\left(r^{2} \varepsilon_{f,V}^{p} x_{f,i}^{p} c_{f}^{p} \right) + \frac{d}{dr}\left(r^{2} \varepsilon_{f,A}^{p} \overrightarrow{N_{f,i}^{p}} \right) \tag{4}$$

Reactor Domain:

$$\varepsilon_{s,V}^{r} \frac{A^{p}}{\varepsilon_{s,V}^{p} V^{p}} \left[\left(\varepsilon_{f,A}^{p} \overrightarrow{N_{f,i}^{p}} \right) \Big|^{z,r^{p}} \right] = \frac{d}{dt}\left(\varepsilon_{f,V}^{r} x_{f,i}^{r} c_{f}^{r} \right) + \varepsilon_{f,A}^{r} \frac{d}{dz}\left(c_{f}^{r} \overrightarrow{v_{f}^{r}} x_{f,i}^{r} + \overrightarrow{n_{f,i}^{r}} \right) \tag{5}$$

Quantification of species transport inside the catalyst is carried out by using the DGM. In general, the most industrial multiphase reactors run under the reactions condition involving more than two species. Thus, the modeling of the complicated multi-component systems necessitates to use advanced diffusion such as the DGM that enable to achieve the desired level of accuracy in modeling of the transport mechanisms and reaction kinetics**.** DGM accounts 3 transport mechanisms; (1) continuum-or-regular transport: the species in the system gains the motion due to concentration variations, derived using the MSM. (2) viscous diffusion-or-convection: pressure variations causes the motion for species. (3) Knudsen diffusion: the transport mechanism defined as the motion of species by concentration variations in the presence of small pore walls. Thermal diffusion is not took into account in this study (da Cruz *et al.* 2017). The resulting DGM is:

$$-\frac{1}{\sum_{j=1}^{N_s} c_{j}} \sum_{\substack{j=1 \\ j \neq i,p}}^{N_s} \left(\frac{c_{j}}{D_{ij}^{eff}} \overrightarrow{N_{i}} - \frac{c_{j}}{D_{ij}^{eff}} \overrightarrow{N_{j}} \right) - \frac{\overrightarrow{N_{i}}}{D_{iK}^{eff}} = \vec{\nabla} c_{i} + \frac{c_{i}}{\sum_{i=1}^{N_s} c_{i}\, RT} \left(1 + \frac{P}{D_{iK}^{eff}} \frac{B_{O}}{\mu_{f}} \right) \vec{\nabla} P \tag{6}$$

The combined molar fluxes $\overrightarrow{N_i}\ i=1,N_s$, combined mass fluxes $\overrightarrow{J_i}\ i=1,N_s$, and velocities $\overrightarrow{v_i}\ i=1,N_s$ for the ith species, are defined as $\overrightarrow{N_i}=c_i\overrightarrow{v_i}\ i=1,N_s$, $\overrightarrow{J_i}=M_ic_i\overrightarrow{v_i}\ i=1,N_s$. By defining the gas mixture's molar average velocity $\vec{v}=\sum_{i=1}^{N_s}\frac{c_i}{\sum_{j=1}^{N_s}c_j}\overrightarrow{v_i}$ and average mass velocity $\vec{u}=\sum_{i=1}^{N_s}\frac{M_ic_i}{\sum_{j=1}^{N_s}M_jc_j}\overrightarrow{v_i}$, one can decompose the combined molar (mass) fluxes into convective $c_i\vec{v}\ i=1,N_s$ ($M_ic_i\vec{u}\ i=1,N_s$) and diffusive $\overrightarrow{n_i}=c_i\left(\overrightarrow{v_i}-\vec{v}\right)i=1,N_s$ ($\overrightarrow{j_i}=M_ic_i\left(\overrightarrow{v_i}-\vec{u}\right)i=1,N_s$) components, as follows:

$$\overrightarrow{n_i}=c_i\left(\overrightarrow{v_i}-\vec{v}\right)=\overrightarrow{N_i}-c_i\vec{v}=\overrightarrow{N_i}-c_i\sum_{i=1}^{N_s}\frac{c_i}{\sum_{j=1}^{N_s}c_j}\overrightarrow{v_i}\ i=1,N_s$$

$$\overrightarrow{j_i}=M_ic_i\left(\overrightarrow{v_i}-\vec{u}\right)=\overrightarrow{J_i}-M_ic_i\vec{u}=\overrightarrow{n_i}-M_ic_i\sum_{i=1}^{N}\frac{M_ic_i}{\sum_{j=1}^{N}M_jc_j}\overrightarrow{v_j}\ i=1,N_s$$

The application considered here involves five species, $i=CO,CO_2,H_2O,H_2,CH_4$, and the DGM can be written in matrix equation form as:

$$\begin{bmatrix}\overrightarrow{N_1}\\ \overrightarrow{N_2}\\ \overrightarrow{N_3}\\ \overrightarrow{N_4}\\ \overrightarrow{N_5}\end{bmatrix}=-\underbrace{\begin{bmatrix}\left(\frac{\sum_{i=2}^{5}\frac{c_i}{D_{1i}^{eff}}}{\sum_{j=1}^{5}c_j}+\frac{1}{D_{1K}^{eff}}\right) & \frac{-c_1}{D_{12}^{eff}\sum_{j=1}^{5}c_j} & \frac{-c_1}{D_{13}^{eff}\sum_{j=1}^{5}c_j} & \frac{-c_1}{D_{14}^{eff}\sum_{j=1}^{5}c_j} & \frac{-c_1}{D_{15}^{eff}\sum_{j=1}^{5}c_j}\\ \frac{-c_2}{D_{21}^{eff}\sum_{j=1}^{5}c_j} & \left(\frac{\sum_{\substack{i=1\\ i\neq 2}}^{5}\frac{c_i}{D_{2i}^{eff}}}{\sum_{j=1}^{5}c_j}+\frac{1}{D_{2K}^{eff}}\right) & \frac{-c_2}{D_{23}^{eff}\sum_{j=1}^{5}c_j} & \frac{-c_2}{D_{24}^{eff}\sum_{j=1}^{5}c_j} & \frac{-c_2}{D_{25}^{eff}\sum_{j=1}^{5}c_j}\\ \frac{-c_3}{D_{31}^{eff}\sum_{j=1}^{5}c_j} & \frac{-c_3}{D_{32}^{eff}\sum_{j=1}^{5}c_j} & \left(\frac{\sum_{\substack{i=1\\ i\neq 3}}^{5}\frac{c_i}{D_{3i}^{eff}}}{\sum_{j=1}^{5}c_j}+\frac{1}{D_{3K}^{eff}}\right) & \frac{-c_3}{D_{34}^{eff}\sum_{j=1}^{5}c_j} & \frac{-c_3}{D_{35}^{eff}\sum_{j=1}^{5}c_j}\\ \frac{-c_4}{D_{41}^{eff}\sum_{j=1}^{5}c_j} & \frac{-c_4}{D_{42}^{eff}\sum_{j=1}^{5}c_j} & \frac{-c_4}{D_{43}^{eff}\sum_{j=1}^{5}c_j} & \left(\frac{\sum_{\substack{i=1\\ i\neq 4}}^{5}\frac{c_i}{D_{4i}^{eff}}}{\sum_{j=1}^{5}c_j}+\frac{1}{D_{4K}^{eff}}\right) & \frac{-c_4}{D_{45}^{eff}\sum_{j=1}^{5}c_j}\\ \frac{-c_5}{D_{51}^{eff}\sum_{j=1}^{5}c_j} & \frac{-c_5}{D_{52}^{eff}\sum_{j=1}^{5}c_j} & \frac{-c_5}{D_{53}^{eff}\sum_{j=1}^{5}c_j} & \frac{-c_5}{D_{54}^{eff}\sum_{j=1}^{5}c_j} & \left(\frac{\sum_{\substack{i=1\\ i\neq 5}}^{5}\frac{c_i}{D_{5i}^{eff}}}{\sum_{j=1}^{5}c_j}+\frac{1}{D_{5K}^{eff}}\right)\end{bmatrix}^{-1}}_{D^{DGM}}\cdot\underbrace{\begin{bmatrix}\vec{\nabla}c_1+\frac{c_1}{\sum_{j=1}^{N_s}c_jRT}\left(1+\frac{P}{D_{1K}^{eff}}\frac{B_O}{\mu_f}\right)\vec{\nabla}P\\ \vec{\nabla}c_2+\frac{c_2}{\sum_{j=1}^{N_s}c_jRT}\left(1+\frac{P}{D_{2K}^{eff}}\frac{B_O}{\mu_f}\right)\vec{\nabla}P\\ \vec{\nabla}c_3+\frac{c_3}{\sum_{j=1}^{N_s}c_jRT}\left(1+\frac{P}{D_{3K}^{eff}}\frac{B_O}{\mu_f}\right)\vec{\nabla}P\\ \vec{\nabla}c_4+\frac{c_4}{\sum_{j=1}^{N_s}c_jRT}\left(1+\frac{P}{D_{iK}^{eff}}\frac{B_O}{\mu_f}\right)\vec{\nabla}P\\ \vec{\nabla}c_5+\frac{c_5}{\sum_{j=1}^{N_s}c_jRT}\left(1+\frac{P}{D_{5K}^{eff}}\frac{B_O}{\mu_f}\right)\vec{\nabla}P\end{bmatrix}}_{\vec{\nabla}x}$$

Then, a DGM effective diffusivity matrix can be described as D^{DGM} and result to the equation:

$$\overrightarrow{N}=-D^{DGM}\cdot\vec{\nabla}x \tag{7}$$

At moderate pressures, the regular diffusion, effective diffusion coefficients $D_{ij}^{eff}\ i=1,N;\ j=1,N;\ j\neq i$ used in the drived equations, are estimated by Chapman-Enskog theory. The equations derived by Poling, Praunitz and O'Connell are used to calculate the binary diffusion coefficient for polar and non-polar gas mixtures (da Cruz *et al.* 2017). The identicalness of Stefan-Maxwell diffusivities and the binary diffusivities For ideal gas mixtures are reported in the literature (Rout and Jakobsen 2015).

For the reactor-fluid subsystem, MSM can be defined by Eq. (8) to quantify the diffusive flux $\overrightarrow{j_{f,i}^{r}}$:

$$\sum_{j=1}^{\upsilon}\left[\frac{x_{f,i}^{r}\,x_{f,j}^{r}}{D_{ij}}\left(\frac{1}{\rho_{f,j}^{r}}\overrightarrow{j_{f,j}^{r}}-\frac{1}{\rho_{f,i}^{r}}\overrightarrow{j_{f,i}^{r}}\right)\right]= \vec{\nabla}x_{f,i}^{r}+\left(\frac{x_{f,i}^{r}-w_{f,i}^{r}}{p^{r}}\right)\frac{d}{dz}p_{f}^{r}+\sum_{j=1}^{\upsilon}\left[\frac{x_{f,i}^{r}\,x_{f,j}^{r}}{\rho_{f}^{r}D_{ij}^{r}}\left(\frac{\tilde{D}_{i}^{r}}{w_{f,i}^{r}}-\frac{\tilde{D}_{j}^{r}}{w_{f,j}^{r}}\right)\right]\frac{1}{T_{f}^{r}}\frac{d}{dz}T_{f}^{r} \tag{8}$$

The cross-sectional averaged-momentum equation can be shown as (Rout and Jakobsen 2015):

$$\frac{\partial}{\partial t}\left(\rho_{f}^{r}\overrightarrow{v_{f}^{r}}\right)+\vec{\nabla}\cdot\left(\frac{\rho_{f}^{r}\overrightarrow{v_{f}^{r}}\overrightarrow{v_{f}^{r}}}{\varepsilon_{v}^{r}}\right)= \varepsilon_{v}^{r}\vec{\nabla}p_{f}^{r}+\varepsilon_{v}^{r}\left(K_{D}\overrightarrow{v_{f}^{r}}+K_{v}\overrightarrow{v_{f}^{r}}^{2}\right) \tag{9}$$

However, the momentum equation can be reduced to the following form:

$$\vec{\nabla}p_{f}^{r}=-K_{D}\overrightarrow{v_{f}^{r}}-K_{v}\overrightarrow{v_{f}^{r}}^{2}= \frac{d}{dz}p_{f}^{r}=-150\frac{\mu_{f}^{r}\left(1-\varepsilon_{V}^{r}\right)^{2}}{\left(\varepsilon_{V}^{r}\right)^{3}d_{p}^{\,2}}-1.75\frac{\left(1-\varepsilon_{V}^{r}\right)}{\left(\varepsilon_{V}^{r}\right)^{3}d_{p}}\rho_{f}^{r}\overrightarrow{v_{f}^{r}}\overrightarrow{v_{f}^{r}} \tag{10}$$

where K_D and K_V are constants for the viscous and kinetic pressure drop. The addition of the DGM for all species in the system results a source term for the momentum conservation inside the catalyst.

A high heat transfer coefficient is observed inside of the catalyst due to the proximity the solid and fluid phases which results a common temperature T^{p} for the pellet's solid-fluid combined system. The resulting combined energy conservation equation is dedicated by Eq. (11).

$$\left\{\begin{array}{l}\left\{\frac{d}{dz}\left[\left(\varepsilon_{f,A}^{p}k_{f}^{p}+\varepsilon_{s,A}^{p}k_{s}^{p}\right)\frac{d}{dz}T^{p}\right]\right\}= \\ \left\{-\sum_{i=1}^{\upsilon}\tilde{h}_{i}^{p}R_{f,i}^{p}\right\}\end{array}\right. \left\{\begin{array}{l}\left\{\left[\varepsilon_{s,V}^{p}\rho_{s}^{p}C_{V,s}^{p}+\sum_{i=1}^{\upsilon}\varepsilon_{f,V}^{p}\rho_{f}^{p}\left(c_{f,i}^{p}C_{P,i}^{p}\right)\right]\frac{dT^{p}}{dt}\right\} \\ \left\{+\left[\sum_{i=1}^{\upsilon}\varepsilon_{A}\rho_{f}^{p}\left(c_{f,i}^{p}C_{P,i}^{p}\right)\overrightarrow{v_{f}^{p}}\right]\cdot\frac{d}{dz}T^{p}\right\}\end{array}\right. \tag{11}$$

In this study, the derived energy equation contains three terms which represent heat exchanged between the fluid and solid phases within the reactor domain, Eq. (12): the enthalpy carried by the species' mass flux between the reactor and the pellet domains, Eq. (13); the convective heat flux interchanged between the fluid in the reactor and the catalyst-pellet solid phase, Eq. (14);

$$q_{f\to s}^{r}=q_{m}^{r}+q_{c}^{r} \tag{12}$$

$$q_{m}^{r}=\varepsilon_{s,V}^{r}\left(\frac{A^{p}}{\varepsilon_{s,V}^{p}V^{p}}\right)\sum_{i=1}^{\nu}\left[\left(\frac{1}{M_{i}}\tilde{h}_{f,i}^{r}\varepsilon_{f,A}^{p}\overrightarrow{N_{i}^{p}}\right)\Big|^{CS^{p}}\cdot\vec{n}\right] \tag{13}$$

$$q_{c}^{r}=\varepsilon_{s,V}^{r}\left(\frac{A^{p}}{\varepsilon_{s,V}^{p}V^{p}}\right)\left[\varepsilon_{s,A}^{p}\lambda^{rp}\left(T_{f}^{r}-T^{p}\right)\Big|^{CS^{p}}\right] \tag{14}$$

The resulting energy equation of the reactor-fluid domain is given by Eq. (15).

$$\left\{\begin{array}{l}\left\{-\varepsilon_{s,V}^{r}\left(\frac{A^{p}}{\varepsilon_{s,V}^{p}V^{p}}\right)\sum_{i=1}^{\nu}\left[\left(\frac{1}{M_{i}}\tilde{h}_{f,i}^{r}\varepsilon_{f,A}^{p}\overrightarrow{N_{i}^{p}}\right)\Big|^{z,r^{p}}\right]\right\} \\ \left\{-\varepsilon_{s,V}^{r}\left(\frac{A^{p}}{\varepsilon_{s,V}^{p}V^{p}}\right)\left[\varepsilon_{s,A}^{p}\lambda^{rp}\left(T_{f}^{r}-T^{p}\right)\Big|^{z,r^{p}}\right]\right\} \\ \left\{+\frac{d}{dz}\left(\varepsilon_{f,A}^{r}k_{f}^{r}\frac{d}{dz}T_{f}^{r}\right)\right\}\end{array}\right.= \left\{\begin{array}{l}\left\{\varepsilon_{f,V}^{r}\rho_{f}^{r}\left(\sum_{i=1}^{\upsilon}c_{f,i}^{r}C_{P,i}^{r}\right)\frac{dT_{f}^{r}}{dt}+\right\} \\ \left\{\varepsilon_{f,A}^{r}\rho_{f}^{r}\left(\sum_{i=1}^{\upsilon}c_{f,i}^{r}C_{P,i}^{r}\right)\overrightarrow{v_{f}^{r}}\cdot\frac{d}{dz}T_{f}^{r}\right\}\end{array}\right. \tag{15}$$

The kinetics of the WGS reaction has gained growing interest in recently. There are various studies in the literature and they report various rate expressions and mechanisms of the WGSR such as Langmuir-Hinshelwood, Redox, empirical-power-law etc. When we consider all these, empirical-power-law rate expression is being preferred by most of the studies in literature. Commercial catalyst of Co-Mo/Al_2O_3 for LTSR and commercial catalyst of Fe_2O_3-Cr_2O_3 for HTSR catalyst are used in the simulations. The parameters of the empirical model are obtained based on the experimental results, and the reaction

rate can be described by Arrhenius Law to ensure a prediction the rate of reaction computationally. Table 1 represents empirical power-law rate expression with Arrhenius Law, and reaction and equilibrium equations. The constitutive laws and other model equations can be found in Table 2.

Table 1. Chemical Model Equations.

Reaction Rate:

$$r_j = k_0 exp\left(-\frac{E_a}{RT}\right) P_{CO}^{l} P_{H_2O}^{m} P_{CO_2}^{n} P_{H_2}^{q} \left(1 - \frac{1}{K_{eq}} \cdot \frac{P_{CO_2} \cdot P_{H_2}}{P_{CO} \cdot P_{H_2O}}\right)$$

$$K_{eq} = exp\left(\frac{4577.8}{T} - 4.33\right)$$

Table 2. Constitutive Laws and Other Model Equations.

Ideal Gas Law:

$$P = ZcRT = \frac{Z\rho RT}{M}$$

Definitions:

$$\sum_{j=1}^{n_s} x_j = 1,\ c_{tot} = \sum_{i=1}^{\nu} c_i,\ \sum_{j=1}^{n_s} \overrightarrow{n_j} = 0,\ P = \sum_{j=1}^{n_s} P_i$$

Heat Flux (Fourier's Law):

$$Q = -\lambda \nabla T$$

Interphase Heat Transfer Coefficient Correlation:

$$Nu = 2 + 1.1 Pr^{1/3} Re_p^{\ 0.6}$$

Dimensionless Groups:

$$Nu = \frac{h d_p}{\lambda_g},\ Re_p = \frac{\overline{v_f} \rho_g d_p}{\mu_g},\ Pr = \frac{C_{p,g} \mu_g}{\lambda_g}$$

The viscosity of Gas Mixture:

$$\mu_g = \sum_{i=1}^{N_s} \frac{x_i \mu_i}{\sum_{j=1}^{N_s} x_i \phi_{ij}}, \qquad \phi_{ij} = \frac{\left[1 + \left(\mu_i/\mu_j\right)^{1/2} \left(M_j/M_i\right)^{1/4}\right]^2}{8\left(1 + \left(M_i/M_j\right)\right)^{1/2}}$$

Thermal Conductivity:

$$\lambda_{pellet} = \left(1 - \varepsilon_v\right)\lambda_s + \varepsilon_v \lambda_g$$

$$\lambda_{reactor} = \left(1 - \varepsilon_v\right)\lambda_s + \varepsilon_v \lambda_g,\ \ \lambda_s = \beta_{cat}\lambda_{cat} + \beta_{qua}\lambda_{qua},\ \beta_{cat} + \beta_{qua} = 1$$

Thermal Conductivity of Pure Gases:

$$\lambda_i = A_i + B_i T + C_i T^2 + D_i T^3$$

Thermal Conductivity of Gas Mixture:

$$\lambda_g = \sum_{i=1}^{N_s} \frac{x_i \lambda_i}{\sum_{j=1}^{N_s} x_i \phi_{ij}}, \qquad \phi_{ij} = \frac{\left[1 + \left(\mu_i/\mu_j\right)^{1/2} \left(M_j/M_i\right)^{1/4}\right]^2}{8\left(1 + \left(M_i/M_j\right)\right)^{1/2}}$$

The effective axial conductivity:

$$\frac{\lambda_z}{\lambda_g} = \frac{\lambda_z^0}{\lambda_g} + 0.75(Pr)\left(Re_p\right),$$

$$\frac{\lambda_z^0}{\lambda_g} = \varepsilon_v^r + \frac{1 - \varepsilon_v^r}{0.139\varepsilon_v^r - 0.0339 + \frac{2}{3}\left(\frac{\lambda_g}{\lambda_p}\right)}$$

Specific Heat Capacity of Pure Gases:

$$C_i = a_{0,i} + a_{1,i}t + a_{2,i}t^2 + a_{3,i}t^3 + a_{4,i}/t^2,\ \ t = \left(T/1000\right)$$

Specific Heat Capacity of Gas Mixture:

$$C_{p,g} = \sum_{i=1}^{N_s} \frac{x_i M_i C_i}{\sum_{j=1}^{N_s} x_i M_i}$$

Standard Enthalpy of Gases:

$$H_i = H^0 + a_{0,i}t + a_{1,i}\frac{t^2}{2} + a_{2,i}\frac{t^3}{3} + a_{3,i}\frac{t^4}{4} - \frac{a_{4,i}}{t} + a_{5,i} - a_{6,i},\ \ t = \left(T/1000\right)$$

4. Results and Discussion

As mentioned before, the objective of this study is to demonstrate the capability of advanced and detailed numerical modeling and simulation the system (HTSR+LTSR in series) to characterize the behavior of H_2 generation process. In both pellet and reactor scales, RTT-based derived model equations solved simultaneously by Finite Element Method to evaluate the species composition, pressure, temperature, velocity, diffusion fluxes, heat fluxes and convection. To obtain the accurate and reliable model equations, the multi-scale modeling approach is applied in this work. A typical syngas composition of coal/oxygen-blown gasifier off-gas, (H_2/CO/H_2O/CO_2/CH_4) = (2.7637/1.00/a/2.1528/0.84475), used in the simulations, where 1<a<6. Table 3 shows the parameters used in the solution of the catalyst pellet and reactor scales' model equations. Thermal conductivity of the spherical pellet and the gas mixture, specific heat capacity of the gas mixture and standard enthalpies of the gases varies with temperature.

Table 3. HTSR and LTSR Parameters for Simulations.

Parameter	*Value (LTSR)*	*Value (HTSR)*	*Dimension*
Catalyst density	592.68	1008	kg/m^3
Pellet void fraction	0.35	0.35	-
Pellet radius	0.004	0.004	m
Surface area of catalyst	$160*10^3$	$160*10^3$	m^2/g
Pore volume of catalyst	$0.55*10^{-6}$	$0.55*10^{-6}$	m^3/g
Tortuosity	2.8121	2.8121	-
Mean pore diameter	$6.3*10^{-9}$	$6.3*10^{-9}$	m
Inlet pressure	30	40	bar
Inlet temperature	493	573	K
Reactor void fraction	0.7	0.7	-
Chemical-model parameters			
l	0.8	0.74	-
m	0.29	0.47	-
n	-0.07	-0.18	-
q	0	0	-
k_0	6.3	2623.4	$LTSR: mol/atm^{l+m+n+q}\cdot h\cdot g$ $HTSR: \left(m^3/mol\right)^{l+n+m+q}\cdot s^{-1}$
E_a	5.9	80	$LTSR: kcal/mol$ $HTSR: kJ/mol$

4.1. Application of the Multi-scale Model to Industrial-Scale IGCC Plant's Reaction System (the HTSR and he LTSR in series).

The integrated gasification combined cycle-IGCC produces electricity from a solid or liquid fuel. IGCC power plants have similar technology as modern gas fired power plants. IGCC power plants are widely considered being a promising and clean power generation technology. Initial step in IGCC is converting the fuel to syngas which is a mixture of H_2 and CO. Hydrogen production from syngas can be enhanced by the exothermic shift reaction. In the conventional method, WGS catalysts operated sequentially in two stages at two different temperature levels in the presence of H_2S followed by separation of the CO_2 from the hydrogen. In the final stage, a combined cycle power block (a gas turbine + a steam turbine process) is used to generate electricity.

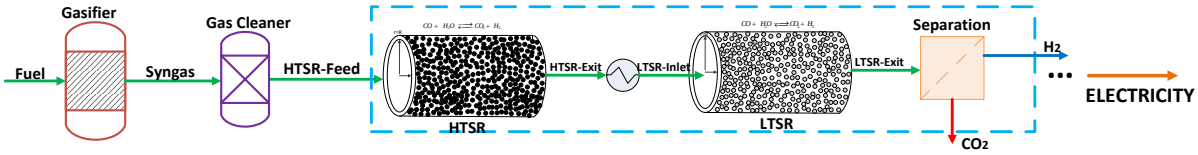

Figure 1. Representation of hydrogen-based IGCC power plant design.

4.1.1. Catalyst-Pellet Scale Results

By using the developed multi-scale model calculations pressure and temperature profiles evaluations of both LTSR and HTSR catalysts along the pellet radius were performed for different operating conditions. These results confirm that there is very small pressure and temperature variation between the pellet surface and center. These results confirm that the general assumptions of the uniform pressure and temperature across the pellet in industry and academic research. These small temperature and pressure changes inside the catalyst do not significantly influence the reaction kinetics. As a conclusion, it is acceptable to consider that the catalyst has uniform temperature profile and isobaric condition along the radius. These results will assist to obtain faster convergence for heterogeneous reactor studies in industry and academia.

The local effect of the catalyst's features such as mean pore diameter, volumetric porosity and tortuosity was studied by simulations. As expected, the reaction rate is proportional to mean pore diameter and pellet's volumetric porosity increase. Due to having the nature of the unchanging total

mole numbers (being steady sate), along the pellet radial position, it is necessary to obtain the result of being zero in sum of the species' molar fluxes- mass averaged velocities. These conditions fulfil consistency checks of the simulation results and the employed numerical accuracy. In this study, the mass/mole averaged velocities and total flux sum for the mole-based DGM at steady-state conditions were found to be zero as expected. Based on the obtained results, it is reasonable to say that the diffusion term evidently dominates over the convective term. Thus, neglection of the species' convective flux contribution in the calculations is an acceptable conclusion.

4.1.2. Reactor Scale Results

Most of the existing studies related to WGSR in literature assumes constant effectiveness factors of the catalysts along the reactors. However, in this study, the DGM is used to evaluate the effectiveness factor of the catalysts for throughout the system reactors' axes. Due to the WGSR stoichiometric feature, the multi-scale model-based calculation of the effectiveness factors results same value for all reaction related species, CO-CO_2-H_2-H_2O. Figure 4 demonstrates that the effectiveness factor declines throughout for both the HTSR and LTSR (adiabatic reactors) lengths. The reason for this decline can be explained as that because of the exothermicity of the WGSR, the acceleration on the intrinsic kinetics of the reaction occurs through the axes of the both reactors (HSTR-LTSR due to temperature increments which causes more increment in the denominator of effectiveness-factor's equation respect to its numerator.

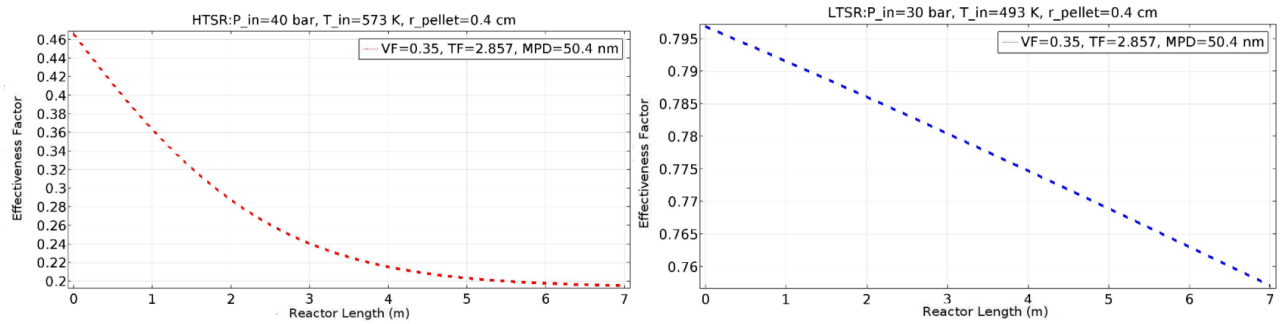

Figure 2. Effectiveness factor axial profiles for HTSR-Left and LTSR-Right, VF: void fraction, MPD: mean pore diameter and TF: Tortuosity Factor.

The temperature profiles along the both reactors' length are shown in Figure 5. Multi-scale modeling approach enables to quantify the temperature evaluations separately for all domains in both reactors. Throughout the reactor lengths for HTSR and LTSR, the observed maximum-minimum temperature differences between the bulk gas phase and catalyst pellet are 1.2-0.02 K for HTSR and 0.85-0.285 K for LTSR, respectively.

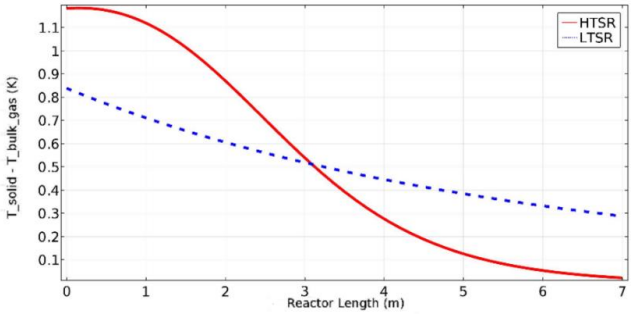

Figure 3. Axial temperature profiles (temperature difference between catalyst pellet and reactor bulk gas) for HTSR and LTSR at steady-state conditions.

For industrial applications, a integrated HTSR and LTSR system is preferred method to achieve a desired high conversions from the WGSR. Figure 6 shows the conversion evaluation of this system for the industrial scale process. The CO conversion is nearly completed or reached the high levels for the selected starting reaction temperature of the LTSR (493 K) and HTSR (573 K). In general, industrially, observed CO conversion by using HTSR and LTSR system is above 97% and as can be seen in Figure 6, similar results achieved in this study by using multi-scale modeling approach. Operating both HTSR and LTSR at higher pressure and H_2O/CO ratios promote to reach complete or higher-level conversions.

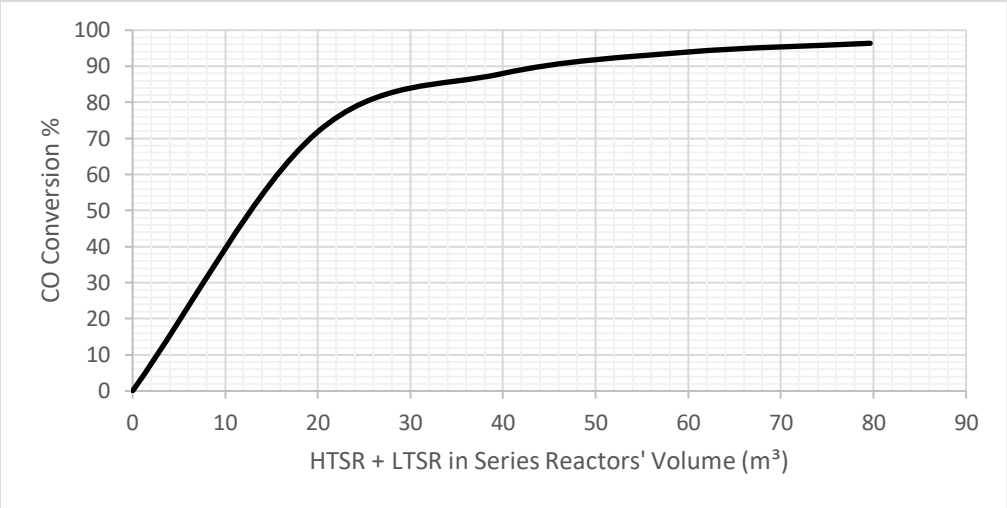

Figure 4. Combined conversion evaluation along the combined reactor's length for industrial scale application.

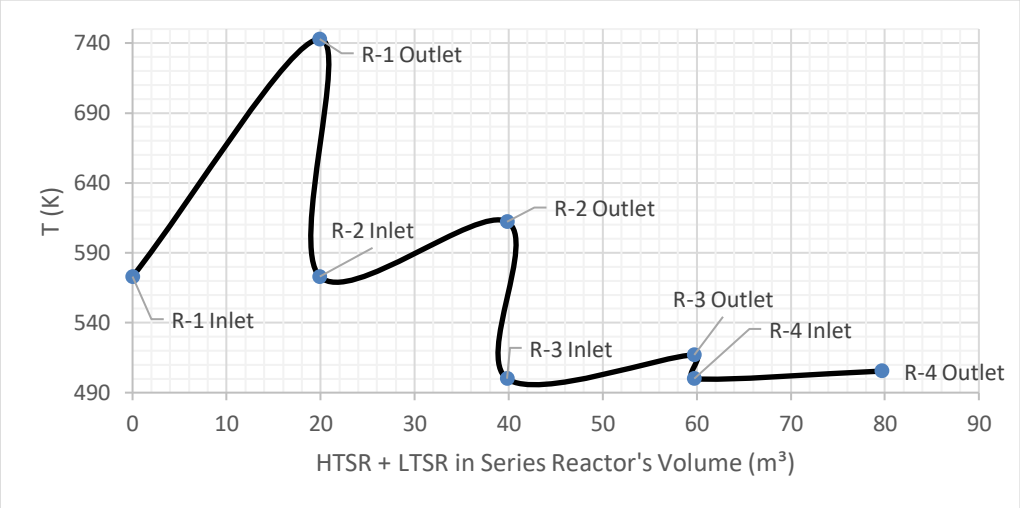

Figure 5. Combined system's (HTSR+Cooling+LTSR) temperature profiles evaluations along the combined reactor's length for industrial scale application.

Figure 7 shows the temperature profiles' evaluations along the combined reactor's length for the combined HTSR and LTSR system. In this study, 2 HTSR and 2 LTSR in series (industrial design) were simulated. In Figure 7, R-1 and R-2 indicates HTSR-1 and HSTR-2 while R-3 and R-4 represent LTSR-1 and LTSR-2 and all reactors operates adiabatically. R-1 and R-2 starting operating temperatures is 573 K while R-3 and R-4 is 493 K and multi-scale model captured outlet temperatures are shown in Figure 7.

5. Conclusions

A multi-scale modeling and simulation of the LTSR and HTSR has been individually performed to investigate the mass and heat transfer effects on the

detailed behavior of the reactions in the catalyst beds and combined process. The developed multi-scale model is applicable to any catalyst for which kinetic data are available. A comparative investigation of two diffusion rate expressions Knudsen diffusion only, and both Knudsen and normal diffusion performed to determine the limiting diffusion step for the considered conditions and catalyst. As a result, it was found that Knudsen diffusivity is the limiting diffusion step for the considered conditions and catalysts. The influence of operating conditions and design parameters on the reactor performance is mainly addressed. The local influence of the catalyst pellet design parameters have been investigated using the rigorous dusty gas model (DGM), Chapman-Enskog models, and finite element method (FEM) theory. The single pellet simulations show us that the simplification on the application of the Dusty Gas Model (DGM), and conceding the uniformity on temperature and pressure gradient inside the spherical pellet are acceptable assumptions. Calculated and comparative temperature profiles of catalyst-pellet and bulk gas phase along the reactors were addressed. Then, the application of the Multi-scale Model to Industrial Scale IGCC Plant's Reaction System was performed, and it was demonstrated that the developed multi-scale model-based simulation outcomes result a very good match with real plant's operating conditions.

6. Notation

English Symbols

$A^p\left(m^2\ of\ domain\ p\right) = the\ control\ surface\ area\ of\ pellet\ domain.$

$A_c^r\left(m^2\right) = the\ tubular\ reactor's\ reactor\ cross\ section\ area.$

$$c_{\gamma,i}^{\alpha}(molar\ density) = \frac{mole\ of\ species\ i\ in\ phase\ \gamma\ within\ domain\ \alpha}{m^3\ of\ phase\ \gamma\ within\ domain\ \alpha}$$

$$C_{P,i}^{\alpha}(molar\ specific\ heat\ at\ constant\ pressure) = \frac{J\ of\ species\ i\ in\ phase\ \gamma\ within\ domain\ \alpha}{\left(mol\cdot K\right)of\ the\ i^{th}\ component\ of\ phase\ \gamma\ within\ domain\ \alpha}$$

$$C_V^{\alpha}(molar\ specific\ heat\ at\ constant\ volume) = \left(\frac{J\ \ phase\ s\ within\ domain\ \alpha}{\left(mol\cdot K\right)of\ phase\ s\ within\ domain\ \alpha}\right)$$

$$CS^{\alpha}(Control\ surface) = m^2\ of\ domain\ \alpha$$

$$CV^{\alpha}(Control\ volume) = m^3\ of\ domain\ \alpha$$

$$D_{ij}^{\alpha}(binary\ diffusion\ coefficient) = \frac{m^2\ of\ phase\ f\ within\ of\ domain\ \alpha}{s}$$

$$D_{ij}^{eff}(effective\ binary\ diffusion\ coefficient) = \frac{m^2\ of\ domain\ p}{s}$$

$$D_{iK}(Knudsen\ diffusion\ coefficient) = \frac{total\ m^2\ of\ domain\ p}{s}$$

$d^p\left(m\right) = Diameter\ of\ the\ catalytic\ pellet$

$d_{pore}^{p}\left(m\right) = Mean\ pore\ diameter\ in\ domain\ p$

$d^r\left(m\right) = Diameter\ of\ the\ tubular\ reactor$

$$h^{\alpha}\left(Interfacial\ heat\ transfer\ coefficient\right) = \frac{J\ \ from\ phase\ f\ within\ domain\ \alpha}{\left(\left(m^2\cdot K\right)of\ phase\ s\ within\ domain\ \alpha\right)\cdot s}$$

$$H_{\gamma}^{\alpha}(Mass\ specific\ enthalpy) = \frac{J\ of\ phase\ \gamma\ within\ domain\ \alpha}{kg\ of\ phase\ \gamma\ within\ domain\ \alpha}$$

$$\tilde{H}_i^0(standard\ molar\ enthalpy\ of\ formation) = \frac{J\ of\ species\ i\ in\ phase\ f}{mol\ of\ species\ i\ in\ phase\ f}$$

$$\tilde{h}_{\gamma,i}^{\alpha}(molar\ enthalpy) = \left(\frac{J\ \ of\ phase\ \gamma\ within\ domain\ \alpha}{mol\ of\ phase\ \gamma\ within\ domain\ \alpha}\right)$$

$$k_{\gamma}^{\alpha}(Thermal\ conductivity) = \frac{J\ \ of\ phase\ \gamma\ within\ domain\ \alpha}{\left(\left(m\cdot K\right)of\ phase\ \gamma\ within\ domain\ \alpha\right)\cdot s}$$

$$\overrightarrow{j_{\gamma,i}^{\alpha}}(diffusion\ mass\ flux) = \frac{mol\ of\ species\ i\ \ in\ phase\ \gamma\ within\ domain\ \alpha}{\left(m^2\ of\ \ phase\ \gamma\ within\ domain\ \alpha\right)\cdot s}$$

$$\overrightarrow{J_{\gamma,i}^{\alpha}}(combined\ \ diffusion-convection\ mass\ flux) = \frac{mol\ of\ species\ i\ \ in\ phase\ \gamma\ within\ domain\ \alpha}{\left(m^2\ of\ \ phase\ \gamma\ within\ domain\ \alpha\right)\cdot s}$$

$L^r\left(m\right) = Length\ of\ \ the\ tubular\ reactor$

$$M_i(molar\ \ mass) = \frac{kg\ of\ i}{mol\ of\ i}$$

$\overrightarrow{n}\left(dimensionless\right) =$
$Unit\ vector\ direction\ of\ \ the\ differential\ area\ dA of\ \ the CS$

$$\overrightarrow{n_{\gamma,i}^{\alpha}}(diffusion\ molar\ \ flux) = \frac{kg\ of\ species\ i\ \ in\ phase\ \gamma\ within\ domain\ \alpha}{\left(m^2\ of\ \ phase\ \gamma\ within\ domain\ \alpha\right)\cdot s}$$

$$\overrightarrow{N_{\gamma,i}^{\alpha}}(combined\ \ diffusion-convection\ mass\ \ flux) = \frac{kg\ of\ species\ i\ \ in\ \ phase\ \gamma\ within\ domain\ \alpha}{\left(m^2\ of\ \ phase\ \gamma\ within\ domain\ \alpha\right)\cdot s}$$

$$p^{\alpha}(Pressure) = \frac{J\ \ of\ phase\ f\ within\ domain\ \alpha}{m^3\ of\ \ phase\ f\ within\ domain\ \alpha}$$

$$\overrightarrow{Q_{\gamma}^{\alpha}}(Heat\ \ flux) = \frac{J\ \ of\ \ phase\ \gamma\ within\ domain\ \alpha}{\left(m^2\ of\ \ phase\ \gamma\ within\ domain\ \alpha\right)\cdot s}$$

$$\overrightarrow{q_{f\to s}^{\alpha}}(Heat\ \ transfer) = \frac{J\ \ from\ phase\ f\ to\ s\ within\ domain\ \alpha}{\left(m^3\ of\ domain\ \alpha\right)\cdot s}$$

$$R_{\gamma,i}^{\alpha}(volumetric\ generation\ rate) = \frac{mols\ of\ species\ i\ in\ phase\ \gamma\ within\ domain\ \alpha}{\left(m^3\ of\ domain\ \alpha\right)\cdot s}$$

$$\bar{R}_{f,i}^{p}(generation\ rate) = \frac{mols\ of\ species\ i\ in\ phase\ f\ within\ domain\ p}{\left(kg\ of\ phase\ s\ within\ domain\ p\right)\cdot s}$$

$$\tilde{R}(Universal\ gas\ constant) = \frac{J}{mol.K}$$

$$r^{p}(m) = Radius\ of\ the\ pellet$$

$$T_{\gamma}^{\alpha}(K) = Temperature$$

$$T^{p}(K) = Temperature\ of\ the\ pellet$$

$$T^{w}(K) = Temperature\ of\ inner\ wall$$

$$V^{p}(Total\ volume) = m^3\ of\ domain\ p$$

$$\overrightarrow{v_{\gamma}^{\alpha}}\left(\frac{m}{s}\right) = Mass\ average\ velocity$$

$$\overrightarrow{v_{\gamma,i}^{\alpha}}\left(\frac{m}{s}\right) = species\ velocity$$

$$w_{\gamma,i}^{\alpha}(species\ mass\ fraction) = \frac{kg\ of\ species\ i\ in\ phase\ \gamma\ within\ domain\ \alpha}{kg\ of\ phase\ \gamma\ within\ domain\ \alpha}$$

$$x_{\gamma,i}^{\alpha}(species\ molar\ fraction) = \frac{mol\ of\ species\ i\ in\ phase\ \gamma\ within\ domain\ \alpha}{mol\ of\ phase\ \gamma\ within\ domain\ \alpha}$$

Greek symbols:

$$\varepsilon_{\gamma,V}^{\alpha}(Volumetric\ fraction) = \frac{m^3\ of\ phase\ \gamma\ within\ domain\ \alpha}{total\ m^3\ of\ domain\ \alpha}$$

$$\varepsilon_{\gamma,A}^{\alpha}(Surface\ fraction) = \frac{m^2\ of\ phase\ \gamma\ within\ domain\ \alpha}{total\ m^2\ of\ domain\ \alpha}$$

$$\rho_{\gamma}^{\alpha}(Mass\ density) = \frac{kg\ of\ phase\ \gamma\ within\ domain\ \alpha}{m^3\ of\ phase\ \gamma\ within\ domain\ \alpha}$$

$$\rho_{\gamma,i}^{\alpha}(species\ mass\ concentration) = \frac{kg\ of\ species\ i\ in\ phase\ \gamma\ within\ domain\ \alpha}{m^3\ of\ phase\ \gamma\ within\ domain\ \alpha}$$

$$\tau(Tortuosity) = \frac{m\ of\ diffusion\ path\ length\ in\ phase\ f\ within\ domain\ p}{m\ of\ CV\ length\ in\ domain\ p}$$

$$\mu_{f}^{\alpha}(Viscosity) = \frac{kg\ of\ species\ i\ in\ phase\ \gamma\ within\ domain\ \alpha}{\left(m\ of\ phase\ \gamma\ within\ domain\ \alpha\right)\cdot s}$$

$$\upsilon\left(dimensionless\right) = Total\ number\ of\ species\ in\ the\ phase-domain$$

7. References

Abdollahi, M., Yu, J., Hwang, H.T., Liu, P.K., Ciora, R., Sahimi, M., Tsotsis, T.T., 2010. Process intensification in hydrogen production from biomass-derived syngas. *Industrial & Engineering Chemistry Research,* **49**, 10986–10993.

Adrover, M.E., López, E., Borio, D.O., Pedernera, M.N., 2009. Simulation of a membrane reactor for the WGS reaction: Pressure and thermal effects. *Chemical Engineering Journal*, **154**, 196–202.

Chen, W.-H., Lin, M.-R., Jiang, T.L., Chen, M.-H., 2008. Modeling and simulation of hydrogen generation from high-temperature and low-temperature water gas shift reactions. *International Journal of Hydrogen Energy,* **33**, 6644–6656.

da Cruz, F.E., Karagöz, S., Manousiouthakis, V.I., 2017. Parametric Studies of Steam Methane Reforming Using a Multiscale Reactor Model. *Ind. Eng. Chem. Res.*, **56**, 14123–14139.

Ding, O.L., Chan, S.H., 2008. Water–gas shift reaction – A 2-D modeling approach. *International Journal of Hydrogen Energy*, **33**, 4325–4336.

Francesconi, J.A., Mussati, M.C., Aguirre, P.A., 2007. Analysis of design variables for water-gas-shift reactors by model-based optimization. *Journal of Power Sources*, **173**, 467–477.

Froment, G.F., 1974. Fixed bed catalytic reactors. Technological and fundamental design aspects. *Chemie Ingenieur Technik*, **46**, 374–386.

Garshasbi, A., Chen, H., Cao, M., Karagöz, S., Ciora Jr, R.J., Liu, P.K., Manousiouthakis, V.I., Tsotsis, T.T., 2017. Membrane-based reactive separations for process intensification during power generation. *Catalysis Today*, ***331***, 18-29.

Huang, J., Ho, W.W., 2008. Effects of system parameters on the performance of CO2-selective WGS membrane reactor for fuel cells. *Journal of the Chinese Institute of Chemical Engineers*, **39**, 129–136.

Karagöz, S., Chen, H., Cao, M., Tsotsis, T.T., Manousiouthakis, V.I., 2019a. Multiscale model based design of an energy-intensified novel adsorptive reactor process for the water gas shift reaction. *AIChE Journal,* **65**, e16608.

Karagöz, S., Tsotsis, T.T., Manousiouthakis, V.I., 2019b. Multi-scale modeling and simulation of a novel membrane reactor (MR)/adsorptive reactor (AR) process. *Chemical Engineering and Processing - Process Intensification*, **137**, 148–158.

Karagöz, S., da Cruz, F.E., Tsotsis, T.T., Manousiouthakis, V.I., 2018. Multi-scale membrane reactor (MR) modeling and simulation for the water gas shift reaction. *Chemical Engineering and Processing - Process Intensification*, **133**, 245–262.

Karagöz, S., Tsotsis, T.T., Manousiouthakis, V.I., 2020. Multi-scale model based design of membrane reactor/separator processes for intensified hydrogen production through the water gas shift reaction. *International Journal of Hydrogen Energy, Hydrogen separation/purification via membrane technology,* **45**, 7339–7353.

Lim, J.Y., Dennis, J.S., 2012. Modeling reaction and diffusion in a spherical catalyst pellet using multicomponent flux models. *Industrial & Engineering Chemistry Research*, **51**, 15901–15911.

Miller, C.T., Christakos, G., Imhoff, P.T., McBride, J.F., Pedit, J.A., Trangenstein, J.A., 1998. Multiphase flow and transport modeling in heterogeneous porous media: challenges and approaches. *Advances in Water Resources,* **21**, 77–120.

Natesakhawat, S., Wang, X., Zhang, L., Ozkan, U.S., 2006. Development of chromium-free iron-based catalysts for high-temperature water-gas shift reaction. *Journal of Molecular Catalysis A: Chemical,* **260**, 82–94.

Rout, K.R., Jakobsen, H.A., 2015. A numerical study of fixed bed reactor modelling for steam methane reforming process. *The Canadian Journal of Chemical Engineering*, **93**, 1222–1238.

Seo, Y.-S., Seo, D.-J., Seo, Y.-T., Yoon, W.-L., 2006. Investigation of the characteristics of a compact steam reformer integrated with a water-gas shift reactor. *Journal of Power Sources,* **161**, 1208–1216.

Wright, G.T., Edgar, T.F., 1994. Nonlinear model predictive control of a fixed-bed water-gas shift reactor: An experimental study. Computers & Chemical Engineering, *An international journal of computer applications in chemical engineering,* **18**, 83–102.